Dynamic Segmentation of the Cerebral Cortex in MR Data using Implicit Active Contours

Stefan Sokoll[a], Karsten Rink[a*], Klaus Tönnies[a] and André Brechmann[b]

[a]Department of Simulation and Graphics, University of Magdeburg,
[b]Leibniz Institute for Neurobiology, Magdeburg

Abstract. We propose a dynamic coupled-surface level set approach for the segmentation of the cerebral cortex in MR images of the human brain. An iterative scheme for the estimations of local intensity distributions is applied to compensate for artefacts within the data. Results are given for 5 MR data sets acquired on a 3 Tesla Scanner. No pre-processing is required and a constant set of parameters is used for all data sets. We also present a comparison to segmentation results created by the standard neuroimaging software BrainVoyager and show advantages of our approach.

1 Introduction

A precise segmentation of the grey and white matter in anatomical MR data is necessary for a large number of medical applications, e.g. the analysis of functional organisation of cortical areas.

An automatic segmentation of the cortex is difficult as the human brain has a high inter–subject variability, restricting the use of general anatomical knowledge. Furthermore, the image data usually includes a number of artefacts due to magnetic field inhomogeneities, motion and noise. Also, the limited spatial resolution results in partial volume effects which introduce uncertainties in defining the boundaries of the cortex.

Several methods to (semi)automatically estimate gray and white matter volumes in MRI have been applied in recent years [1]. Popular methods estimate the intensity distributions for the various tissue types from the image histogram [2]. These estimates are then used in a following tissue classification or region growing approach [3]. Other methods include the use of active contours and surfaces [4, 5].

2 Method

We propose a dynamic algorithm for the segmentation of the cerebral cortex based on the coupled surface level set approach first proposed by Zeng *et al.* [6] and later adopted by Goldenberg *et al.* [5]. This approach uses two active surfaces for the segmentation of the cortex. While each of the surfaces may evolve according to different features within the data, they have to stay in a predefined normal range to each other given by the estimated cortical thickness.

The level set method was introduced by Osher and Sethian [7] and later adopted to image processing [8]. The basic idea is to calculate the evolution of a closed active contour or surface $\gamma \in \Re^n$ implicitly via a higher dimensional function $\Phi \in \Re^{n+1}$ by assuming that $\gamma(t) = \{\mathbf{x}|\Phi(\mathbf{x}, t) = 0\}$ at each time step t. The method allows for the segmentation of objects whose shape has many degrees of freedom or large variations between data sets.

In the following description of our method, we denote by Ω_{wm} the set of voxels within the inner surface γ_{in}, Ω_{csf} is the set of voxels outside the outer surface γ_{out} and Ω_{gm} are voxels between γ_{in} and γ_{out}. At the end of the segmentation process, voxels $\mathbf{x} \in \Omega_{wm}$ are classified as white matter (WM), $\mathbf{x} \in \Omega_{gm}$ as grey matter (GM) and $\mathbf{x} \in \Omega_{csf}$ as cerebrospinal fluid (CSF) and non-brain-tissue.

It was already mentioned that the original data is affected by magnetic field inhomogeneities. Therefore, each data set is subdivided into cubic divisions D_i of size l^3. It is assumed that inhomogeneities are negligible within each division. All necessary estimations for intensity distributions are made during the propagation process. Since results should be as exact as possible, no preprocessing steps should be performed on the original data. Nevertheless, the data sets have been rotated into the AC/PC-plane (for details see section 3) to be able to compare our results to those obtained by the commercial software BrainVoyagerQX [9].

To start the algorithm, the inner surface γ_{in} needs to be initialised within the white matter. The segmentation result is independent of the location of the initialisation. The outer surface γ_{out} is automatically placed around γ_{in} and

*E-mail: karsten@isg.cs.uni-magdeburg.de

may contain voxels representing grey or white matter. While the distance between both surfaces may change during segmentation, it is set to $3mm$ for initialisation.

No assumptions about image intensities for grey matter, white matter and cerebrospinal fluid are made prior to the segmentation. Intensity distributions for each tissue class are estimated iteratively from the data within the three subdomains for each subdivision D_i. In our algorithm, we assume Gaussian distributions P_{wm} and P_{gm} for white and grey matter, respectively, and a Poisson distribution P_{csf} for the third class containing CSF and non-brain-tissue. Intensities used for the estimate of P_{csf} are limited to grey values $g \in [0, \frac{\mu_{wm}}{2}]$, with μ_{wm} being the mean value of P_{wm}. Especially in the early stages of the segmentation process, it is rather difficult to find a good estimate for P_{csf} since many of the voxels $\mathbf{x} \in \Omega_{csf}$ actually belong to one of the other two distributions. Based on the available data sets, we found $\frac{\mu_{wm}}{2}$ to be an adequate threshold since it is much larger than image intensities usually belonging to CSF and still guarantees only a limited overlap with the other distributions. Also, the estimate for μ_{wm} is reliable from the beginning due to initialisation of the algorithm within the white matter.

We use a reliability measure $R = \min\{R_{ij}, Rji\}$ with

$$R_{ij} = 1 - \sum_{A} P(\mathbf{x}) \qquad A = \{\mathbf{x} | P_i(\mathbf{x}) \leq P_j(\mathbf{x})\} \tag{1}$$

to control if two distributions P_i and P_j, $i, j \in \{wm, gm, csf\}$, are separated well enough within each division that the boundary between these classes may have been found. $R \in [0, 1]$ gives large values if the distributions are well separated and smaller values if they intersect.

The propagation speed is based on the estimates of the intensity distribution on the inside and on the outside of each of the surfaces. To guarantee a smooth transition between neighbouring divisions, the speed of a voxel on the front is not only based on the division it is located in, but also on the 6-neighbourhood of adjacent divisions. For the inner surface, we let

$$M_{in} = \frac{1}{N} \sum_{i=0}^{6} \omega_i (p_i(\mathbf{x}|P_{wm}) - p_i(\mathbf{x}|P_{gm})) \tag{2}$$

and

$$F_{in} = \begin{cases} 1, & \text{if } M_{in} > 0, \\ 0, & \text{otherwise} \end{cases} \tag{3}$$

The weight $\omega_i \in [0, 1]$ for each of the involved divisions D_i is dependent on three properties: the reliability-measure $R = \min\{R_{ij}, R_{ji}\}$, the number of voxels the estimates for the distributions are based on in that division, as well as the distance of the front-voxel $\mathbf{x}$ to the center of that division. That is, ω_i is large if the estimated intensity distributions of division D_i are well separated, the estimates are based on a large number of voxels and the distance of $\mathbf{x}$ to the center of D_i is small. Also note, that the impact of these properties on ω_i is not to be adjusted manually but based on the quality in neighbouring subdivisions.

Likewise, the speed F_{out} for the outer surface is based on

$$M_{out} = \frac{1}{N} \sum_{i=0}^{6} \omega_i (p_i(\mathbf{x}|P_{gm}) - p_i(\mathbf{x}|P_{csf})) \tag{4}$$

The final equation for the coupled surfaces is then given by

$$\frac{\partial \Phi_{in}}{\partial t} = c_{in}(\Phi_{out}) F_{in} |\nabla \Phi_{in}| \tag{5}$$

$$\frac{\partial \Phi_{out}}{\partial t} = c_{out}(\Phi_{in}) F_{out} |\nabla \Phi_{out}| \tag{6}$$

where c_{in} and c_{out} are functions depending on the distance d between Φ_{in} and Φ_{out}. We let

$$c_{in}(d) = \begin{cases} 1, & \text{if } d \geq d_e - d_v, \\ \varepsilon(d), & \text{if } d_e - 2d_v < d < d_e - d_v, \\ 0, & \text{if } d \leq d_e - 2d_v \end{cases} \quad \text{and} \quad c_{out}(d) \begin{cases} 1, & \text{if } d \leq d_e + d_v, \\ \varepsilon(d), & \text{if } d_e + 2d_v > d > d_e + d_v, \\ 0, & \text{if } d \geq d_e + 2d_v. \end{cases} \tag{7}$$

The expected distance d_e between both surfaces is dependent on a cortex thickness map based on [10] that has been incorporated into the algorithm. That is, d_e varies from $2.5mm$ in the occipital cortex to $3.5mm$ in the pre-frontal lobe.

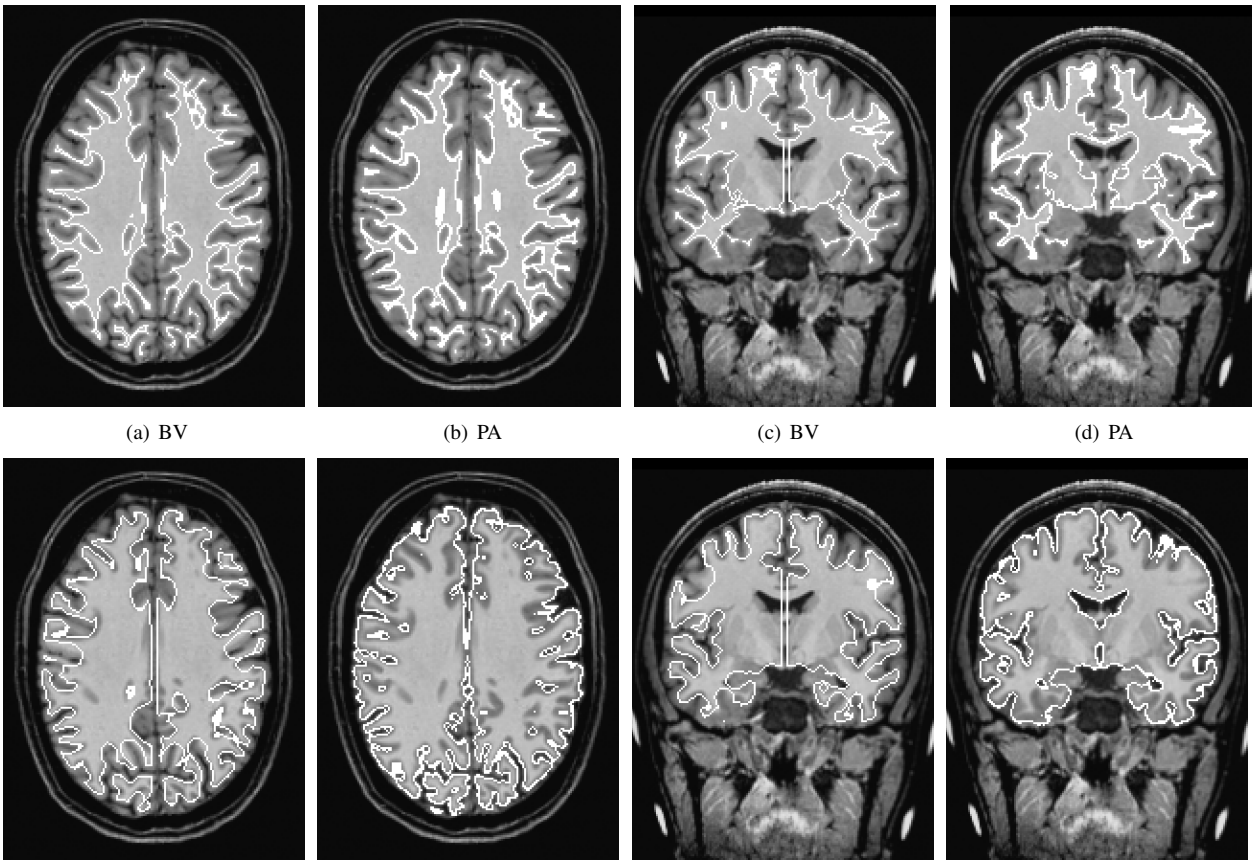

(a) BV (b) PA (c) BV (d) PA

(e) BV (f) PA (g) BV (h) PA

Figure 1. Comparison of segmentation results using BrainVoyager (BV) and our proposed algorithm (PA). The first two columns show examples of axial slices, the last two columns examples of coronal slices. Figs. 1(a)–1(d) depict the inner cortical boundary. Results are similar for both segmentation methods. The boundary between grey matter and cerebrospinal fluid is shown in figs. 1(e)–1(h). Results for both methods vary greatly for this second boundary. While the proposed algorithm actually detects the boundary, BrainVoyager estimates the grey matter by dilation and smoothing of the white matter segmentation which usually results an undersegmentation as well as an inexact boundary.

Φ_{in} is slowed down if the distance between both fronts is too small or Φ_{out} is slowed down if the distance is too large. Both effects only occur if the distance exceeds an accepted variance of $d_v = 0.5mm$. To ensure that c_{in} and c_{out} are smooth functions, we use a monotonically decreasing sigmoid function $\varepsilon(d)$.

Both level set functions Φ_{in} and Φ_{out} are only calculated within a narrow band [11]. To save computational cost, estimates for all intensity distributions are recalculated only when a narrow band is re-initialised.

3 Results

We tested the above algorithm on 5 MR data sets with $1mm$ isotropic resolution acquired on a 3 Tesla Scanner. The quality of the data varied with respect to signal-to-noise ratio and grey level inhomogeneities. The same set of parameters was used for all data sets. The size of the aforementioned subdivisions D_i was $20 \times 20 \times 20$ voxels. Results of the above algorithm have been compared with segmentation results created by BrainVoyager QX, a standard software for the analysis and visualisation of MRI (for details see [9] and `http://www.brainvoyager.com`). These segmentations have been created with interaction by an experienced user and are thus more exact than an automated segmentation using this software. Examples of segmentation results using both algorithms are given in figure 1.

For an analysis using the commercial software, it is necessary to perform an inhomogeneity correction and to rotate the data sets into the AC/PC-plane defined by the interhemispheric fissure and by the *commissura anterior* and *posterior*. Our algorithm was also applied to the AC/PC-rotated data to allow for a comparison of both methods. Due to the rotation, an interpolation of the original data cannot be avoided.

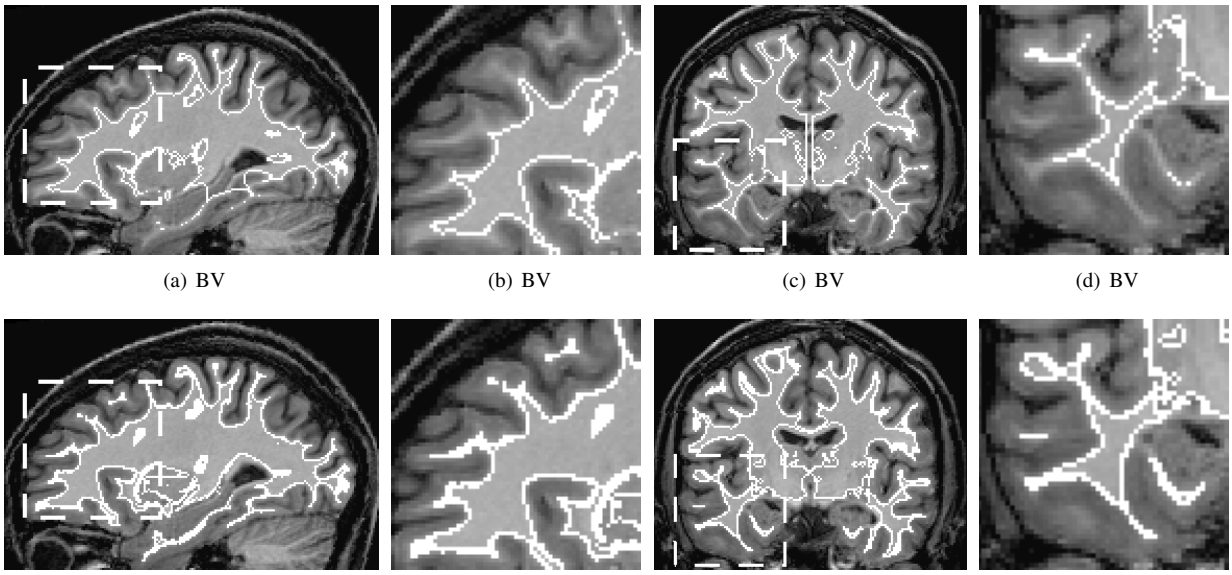

(a) BV (b) BV (c) BV (d) BV

(e) PA (f) PA (g) PA (h) PA

Figure 2. Details of segmentation results for the inner cortical boundary with BrainVoyager and the proposed algorithm. Figures 2(a)–2(d) give results obtained with BrainVoyager. Figures 2(e)–2(h) show results of the proposed methods. Differences are visible in the enlarged areas within the frontal lobe (depicted in the two leftmost columns) and the lower temporal lobe (depicted in the two rightmost columns)

The proposed algorithm gives similar results for the inner cortical surface compared to the segmentation using BrainVoyager on these rotated data sets in most data sets. However, in two data sets our segmentation results were more exact than the results of the commercial software. Examples are given in figure 2. Mean distance as well as Hausdorff distance between both segmentation results for all data sets are given in table 1. A visual inspection by neurobiologists suggests that the boundary between grey and white matter found by our algorithm is usually more exact than the boundary found by BrainVoyager. Thin gyral foldings pose a problem to both segmentation methods due to the aforementioned rotation into the AC/PC-plane. The boundary between grey matter and CSF given by the commercial software is simply an estimate based on the WM/GM-boundary and cortex thickness. Specifically, the inner boundary is dilated and smoothed based on the constraint that no voxels with an image intensity below a constant threshold θ must be included in the grey matter estimate. Therefore, the resulting surface usually underestimates the grey matter. Again, a visual inspection proved the correctness of our segmentation result. Note, that the segmentation result of our algorithm is independent of the location for the initialisation of the contour within the white matter. Also, no user interaction is necessary during the segmentation process.

A number of problems occur with both segmentation methods. Interpolation of the intensities due to the rotation of the data set into the AC/PC-plane might pose a problem as the thin gyral foldings of the human cortex might be additionally distorted. Also, in the presence of strong magnetic field inhomogeneities both methods will give an undersegmentation of the lower temporal lobes and/or the upper part of the frontal lobe (see figure 3). Finally, we cannot guarantee a topologically correct segmentation of the cortex, as neighbouring gyri may not be separable due to partial volume effects (see results for the outer cortical surface in figures 1 and 4).

Finally, we want to mention that the proposed algorithm also allows for the segmentation of the original MR data sets. This is not possible using the commercial software. Obviously, the problem originating from rotation into the AC/PC-plane does not occur on these data sets. Again, a visual inspection by neurobiologists confirms the correctness of the segmentation results. Example slices of segmentation results are given in figure 4.

4 Conclusions

We presented an automated algorithm for the segmentation of grey and white matter in the human brain. The proposed algorithm is independent of any pre-processing of the data sets. It does not require any user-interaction except for initialisation within the white matter. We compared segmentation results of our algorithm to results created by the commercial software BrainVoyager. While results for the boundary between grey and white matter were similar in

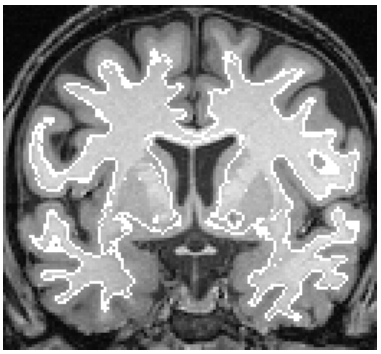

Figure 3. Undersegmentation due to magnetic field inhomogeneities

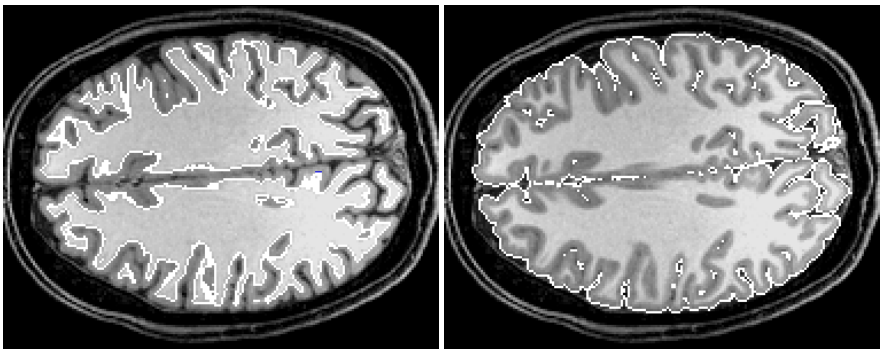

Figure 4. Segmentation example for white matter (left) and grey matter (right) in the original MR data.

data set		lr64	ik41	kc73	lg38	ra41
d_H	inner boundary	8.88	10.86	9.98	9.89	6.90
in mm	outer boundary	9.77	10.55	15.86	12.24	11.17
d_m	inner boundary	0.29	0.68	0.50	0.33	0.32
in mm	outer boundary	1.35	1.11	0.89	0.82	0.85

Table 1. Distances between the segmentation results of the proposed algorithm and the commercial software. Here, d_H denotes the Hausdorff-distance and d_m the mean distance between both surfaces. Segmentation results for white matter are usually similar. Only in data sets 'ik41' and 'kc73' results differ significantly (see figure 2 for details). Large values for d_H are usually the result of a different cut-off at the brainstem.

both algorithms, our method gave much more exact results for the outer cortical surface. A visual inspection by medical experts confirmed the correctness of our results.

Acknowledgements

The authors would like to thank Andreas Fügner for his help concerning the BrainVoyager software and for providing the segmentation results.

References

1. D. L. Pham, C. Xu & J. L. Prince. "Current Methods in Medical Image Segmentation." *Annu Rev Biomed Eng* **2**, pp. 315–337, 2000.
2. J. F. Mangin, O. Coulon & V. Frouin. "Robust Brain Segmentation Using Histogram Scale-Space Analysis and Mathematical Morphology." In *Proc of MICCAI*, pp. 1230–1241. 1998.
3. N. Kriegeskorte & R. Goebel. "An efficient algorithm for topologically correct segmentation of the cortical sheet in anatomical MR volumes." *Neuroimage* **14**, pp. 329–346, 2001.
4. C. Davatzikos & N. Bryan. "Using a deformable surface model to obtain a shape representation of the cortex." *IEEE Trans Med Imag* **15(6)**, pp. 785–795, 1996.
5. R. Goldenberg, R. Kimmel, E. Rivlin et al. "Cortex Segmentation: A Fast Variational Geometric Approach." *IEEE Trans Med Imag* **21(2)**, pp. 1544–1551, 2002.
6. X. Zeng, L. H. Staib, R. T. Schultz et al. "Segmentation and Measurements of the Cortex from 3-D MR Images Using Coupled-Surfaces Propagation." *IEEE Trans Med Imag* **18(10)**, pp. 927–937, 1999.
7. S. Osher & J. A. Sethian. "Fronts Propagating with Curvature Dependent Speed: Algorithms Based on Hamilton-Jacobi Formulation." *J Comput Phys* **79**, pp. 12–49, 1988.
8. R. Malladi, J. A. Sethian & B. Vemuri. "Shape Modelling with Front Propagation: A Level Set Approach." *IEEE Trans Pattern Anal Mach Intell* **17(2)**, pp. 158–175, 1995.
9. R. Goebel. "Brain Voyager 2.0: from 2D to 3D fMRI analysis and visualization." *NeuroImage* **5**, pp. 635, 1997. `http://brainvoyager.com`.
10. B. Fischl & A. Dale. "Measuring the thickness of the human cerebral cortex from magnetic resonance images." *Proc Nat Acad Sci* **97(20)**, pp. 11044–11049, 2000.
11. D. Adalsteinsson & J. A. Sethian. "A Fast Level Set Method for Propagating Interfaces." *J Comput Phys* **118(2)**, pp. 269–277, 1995.